Chapter 11
Nuclear Reaction Analysis

Hans-Werner Becker and Detlef Rogalla

Abstract Nuclear reaction analysis (NRA) is a method utilizing an ion beam from an accelerator to determine the hydrogen content in materials. The hydrogen concentration can be quantified absolute and the method can provide depth profiles in the range up to 2–3 μm with a depth resolution in the range of a few nm. Concentrations of 500 at. ppm are easily measurable and with special efforts sensitivities down to 1 ppm have been achieved. The chapter describes the basic principles of the measurements and data analyses and discusses special cases and complications arising with particular samples or when very low concentrations are to be measured.

Keywords Absolute hydrogen concentration • Accelerator • Background • Beam current • Beam intensity • Beam resolution • Borehole detector • Calibration • Chemical binding • Cross section • Depth information • Depth profiling • Depth resolution • Detector • Deterioration • Doppler broadening • Efficiency • Fluence • Hydrogen concentration • Hydrogen loss • Hydrogen storage material • Low concentration detection • Nuclear reaction analysis • Nuclear resonance reaction • resolution • Resonance • Resonance energy • Stability of samples • Stability of samples • Stopping power • Straggling • Surface • Surface cleaning • Surface peak • Yield • γ-ray detection

11.1 Introduction

The study of hydrogen in materials with a resonance in a nuclear reaction induced by an ion beam from an accelerator is possible because the products of such a reaction (usually α-particles and/or γ-rays) give a unique and quantitative signature of hydrogen present in the sample. Although being a nuclear method, nowadays this technique is so mature and straightforward that in order to be used by the material scientist to analyze his samples and to understand and interpret the results, only little knowledge of nuclear physics is necessary.

H.-W. Becker (✉)
RUBION, Central Unit for Ion Beams and Radioisotopes, Ruhr-University Bochum,
Universitätsstraße. 150, Bochum 44801, Germany
e-mail: hans-werner.becker@rub.de

Nuclear resonance reactions have been used for hydrogen detection in materials already since the 1970s, for example by Leich and Tombrello for the investigation of lunar samples [1]. In this work they used a ^{19}F beam and the resonance at a beam energy of 16.6 MeV. The method became more spread and common in material analysis, when Lanford and coworkers established the resonance at the energy of 6.4 MeV in the reaction induced by a ^{15}N beam [2]. This reaction is nowadays the one mostly used due to the excellent properties of the resonance leading to favorable sensitivity and depth resolution. Therefore in this chapter this reaction is discussed mainly, the principle considerations apply however for other reactions [3–5] as well.

In the case of the ^{15}N method the absolute hydrogen concentration in a sample can be detected down to 500 at. ppm easily with standard techniques and for more sophisticated experimental approaches concentrations down to the 1 at. ppm level have been measured [6]. The hydrogen content is determined depth resolved with a resolution of about 10 nm decreasing somewhat with depth. The maximal probing depth is 2–3 μm. An excellent and very detailed review about the method has been published recently [7].

11.2   The Principle of the Method

11.2.1   Interaction of Ions with Matter

For an understanding of the Nuclear Resonance Reaction Analysis it is necessary to bear in mind the processes that occur when fast ions penetrate into matter. The by far most probable process is the interaction of the ions with the electronic cloud of the atoms mostly with electrons with the smallest binding energies (such as conduction electrons). Each interaction leads to an energy loss of the ion, which reduces the energy successively and brings the ion eventually to a stop within a maximal range. Since the mass difference of ions and electrons is large the energy loss in each collision is small such that this statistical process can be considered in most cases as quasi-continuous. (The Coulomb interaction with the nuclei can be neglected for the ions and energies relevant here.) The energy loss per atomic layer, the stopping cross section ε, is dependent on the element in a sample (i.e. the number of electrons or the atomic numbers Z) and it is given in units of eV/(atoms/cm^2). For compounds the stopping cross section is just the linear combination of the components (Bragg's rule), which is sufficient accurate in most cases, but in some circumstances corrections for the chemical binding need to be applied [8].

Alternatively, the stopping of ions in matter is often described by the so-called stopping power, which is defined as the energy loss per length unit and sometimes there is confusion about these quantities in literature. Though both values describe the same phenomenon, the difference is that the stopping cross section is dependent on the density of the material, which can vary much from element to element and moreover might not be well defined for thin layers or specific sample preparations. There is a vast amount of measured data in literature about the stopping cross

section or the stopping power of many ions in various elements and compounds for a large range of ion energies. These data have been collected in data bases, the most famous and mostly used being SRIM [9], a program which calculates the stopping power of any ion in any sample on a semi-emperical approach taking into account experimental data. Thus, for practical purposes of material analysis stopping cross sections can be considered as something available in the toolbox of the analyst and known with an accuracy of 5–10.

To get a feeling for the stopping cross section one can obtain for example for ^{15}N ions with an energy of 7 MeV in silicon or gold a penetration depth of 5.88 μm and 2.32 μm, a stopping power of 1.38 keV/nm and 3.91 keV/nm and a stopping cross section of 277 eV/(10^{15} atoms/cm^2) and 663 eV/(10^{15} atoms/cm^2) respectively.

11.2.2   Basic Principle of Depth Profiling

Compared to the energy loss process described above, there is a low probability for an ion beam to interact with hydrogen in a sample via the nuclear forces. This nuclear reaction leads to the formation of the intermediate nucleus ^{16}O which in turn decays to an α-particle and an excited ^{12}C which emits a γ-ray of 4.4 MeV. This γ-ray is a unique signature of hydrogen present in the sample and can be used for analysis.

The probability of the reaction as a function of the beam energy is plotted in Fig. 11.1 as a nuclear cross section. This cross section has an isolated and narrow resonance at the beam energy of 6.4 MeV because the energy of the oxygen formed at this beam energy corresponds to an excitation energy state of the oxygen nucleus. This state has a certain lifetime and therefore an energy width associated with it. Several authors [4, 12] have measured this width to be some 1.8 keV or smaller, which is ideal for material analysis purposes and the reason for the high depth resolution of the technique.

The data points in Fig. 11.1 show in the vicinity of the resonance only one point at the maximum because the energy resolution in an accelerator experiment is not good enough for a measurement of such a narrow resonance, which has a Breit-Wigner (i.e. a Lorentzian) shape. Experimentally one observes reactions from the integral over the resonance, from which the cross section at the maximum can be calculated when the width of the resonance is known. The Breit-Wigner curve given in Fig. 11.1 is therefore calculated [10] from measurements integrated over the resonance and the known width. In addition to the resonance at 6.4 MeV there is a small off resonance cross section, which will become important in measurements of very low hydrogen concentrations (see Sect. 11.3.4).

It should be noted that Fig. 11.1 has a logarithmic scale; the cross section at the resonance is more than four orders of magnitude larger than off resonance. Simplifying for a moment the essence of Fig. 11.1 one can say that the resonance occurs at the resonance energy of 6.4 MeV in an energy window of 1.8 keV only. This opens up the possibility for depth profiling.

The principle of the procedure is sketched in Fig. 11.2. If a ^{15}N beam with the energy of the resonance energy enters a sample, the reaction can occur at the
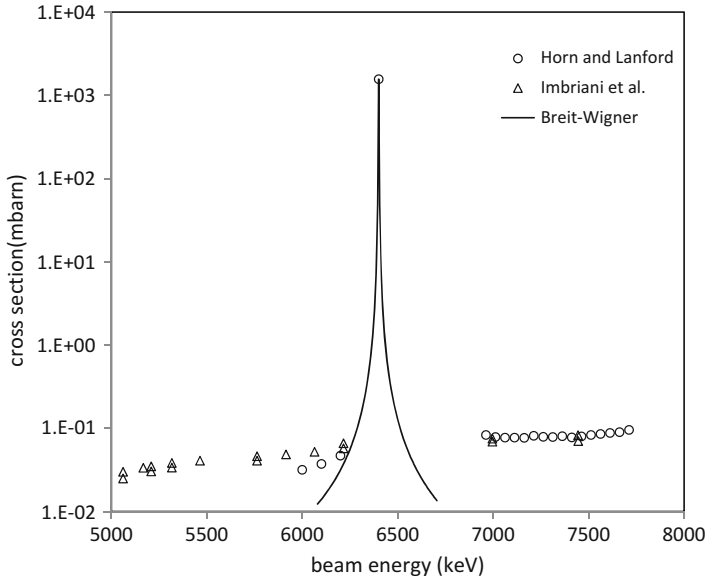
Fig. 11.1 Non-resonant cross section of the ^{1}H(^{15}N,$\alpha\,\gamma$)^{12}C reaction [10, 11]. The *solid line* gives the shape of the resonance with the resonance parameters used in [10]
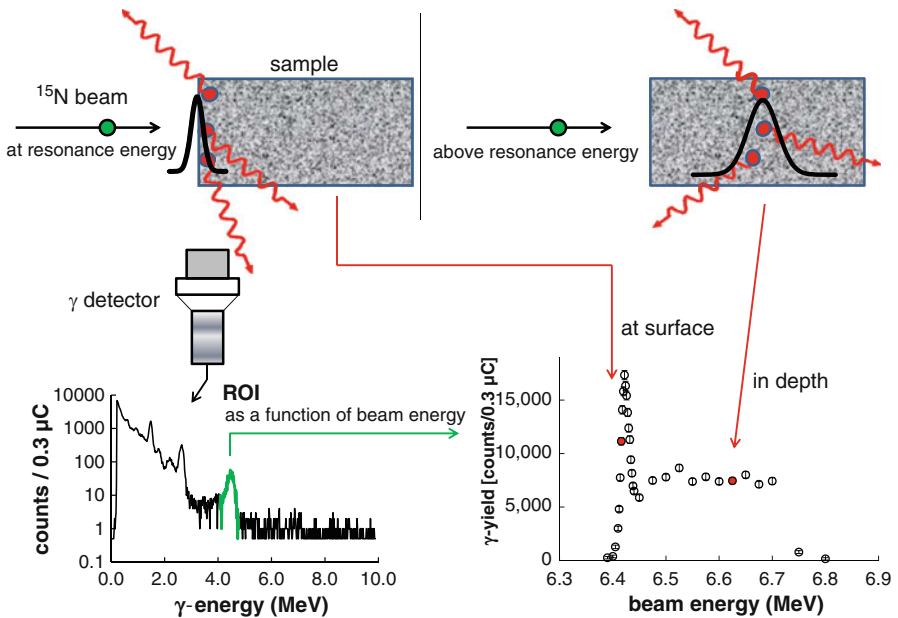

Fig. 11.2 Schematic sketch of depth profiling (see text). The γ-spectrum has been accumulated for a beam charge of 0.3 μC. ROI (region of interest) are the integrated counts over the hydrogen signal (*green peak*). For more details see Sect. 11.3.3

surface. After penetrating a few nm into the sample (depending on the stopping power), the beam has lost more energy than the resonance window and therefore hydrogen cannot be detected. If the beam energy is now increased above the resonance energy, the reaction cannot occur at the surface but after a certain penetration depth, when the ions have lost just enough energy to get into the resonance window. Thus by increasing the beam energy the resonance is visually speaking "shifted" through the sample and probes layers at different depth. The thickness of this layer i.e. the depth resolution is limited by the resonance width and can be estimated from the stopping power (see examples above) to be some 2 nm. However, in reality the depth resolution is poorer, which will be discussed below (Sect. 11.2.5).

The detector in this procedure is for counting the emitted γ-rays only, its resolution is necessary to identify and discriminate the reaction γ-rays against background, but, other than in ERDA (see Chap. 10) or Rutherford-Backscattering-Spectrometry measurements, has no influence on the depth resolution. In most experimental setups today NaI(Tl) detectors or Bithmut Germanate (BGO) detectors are employed because of their high detection efficiency. For a detailed explanation of the spectrum in Fig. 11.2 see Sect. 11.2.5.

The yield Y, i.e. the intensity in the 4.4 MeV γ-line normalized to the number of incident beam particles, is a direct measure for the hydrogen concentration in a sample at a certain depth. The number of beam particles in one measurement is preferably determined by electrical integration of the beam current; the number of particles is then obtained by dividing the accumulated charge by the charge state of the ion beam and the elementary charge. In literature yields are often displayed in units of counts/μC; in comparing different data in this unit one has to consider, which charge state of the ions was used for an experiment. In the following yields are always given in counts per particle μC, where "particle" indicates that the charge is always normalized to the charge state of the ions.

Since the energy of the beam ions is much larger than chemical binding energies the detection process is independent from chemical binding. In this sense the method is "just counting nuclei". This is sometimes advantageous, but on the other hand NRA is not able to give information about the chemical binding.

11.2.3 Determining a Hydrogen Concentration

The total γ-ray yield Y_T from a narrow hydrogen detecting resonance which is defined as the emitted γ-rays per ion beam particles is first of all dependent on the hydrogen concentration of the sample material as well as on the probability of the reaction. Y_T at a certain depth can be written then as:

$$Y_T = R_H \cdot S \cdot \frac{1}{\varepsilon} \qquad (11.1)$$

R_H is the ratio of hydrogen atoms to total atoms of the sample material and corresponds to the hydrogen concentration c_H as defined throughout this book via the relation:

$$R_H = \frac{c_H}{c_H + 1} \tag{11.2}$$

S is a constant representing the probability of the reaction which is here the integral over the resonance cross-section characterized by its height and width sometimes called the strength of the resonance. The third term $1/\varepsilon$ of Eq. (11.1) accounts for the effect of the stopping cross section ε of the sample material. The depth window in which the resonant reaction takes place depends on the energy loss of the ion beam. For a small ε this depth range is larger compared to a case with high stopping cross section and thus containing a larger amount of hydrogen. In other words, the stopping cross section determines the number of hydrogen atoms which are passed by the ions at energies in the small region of the resonance during their deceleration in the sample material.

According to Eq. (11.1) the hydrogen concentration of a sample in a certain depth can be calculated as a function of a measured yield Y and the stopping cross section ε of the sample material. Since γ-detectors in principle detect only a fraction of γ-rays with detection efficiency η the measured yield Y is given by $Y = Y_T \cdot \eta$. A factor $K = 1/(S \cdot \eta)$ can be defined including the strength of the resonance and the detector efficiency. K is a constant for an experimental set up and independent from the sample. Now R_H can be expressed as

$$R_H = Y \cdot K \cdot \varepsilon \tag{11.3}$$

In case of an unknown sample, the determination of the stopping cross section ε requires the knowledge of the hydrogen concentration, which is not known a priori. For small H concentrations the influence of the hydrogen to ε can be neglected, but for higher concentration it becomes significant. One option for calculating R_H is to initially assume a concentration for calculating ε and iteratively recalculate Eq. (11.3) until a consistent result is achieved. Alternatively, a formalism described by Rudolph et al. [13] can be applied. This approach is based on the separation of the total stopping cross section ε of the sample material into the contribution of the hydrogen and the contribution of all other atoms denoted as matrix atoms. It is simply done by adding the stopping cross section of pure hydrogen ε_H and the stopping cross sections of a hydrogen-free matrix ε_M weighted with the individual abundances.

$$\varepsilon = R_H \cdot \varepsilon_H + (1 - R_H)\varepsilon_M \tag{11.4}$$

Combining Eqs. (11.3) and (11.4) one derives to an expression for R_H which does not need an a priori knowledge of the hydrogen concentration.

$$R_H = K \cdot Y \cdot \varepsilon_M \cdot \frac{1}{1 + K \cdot Y \cdot (\varepsilon_M - \varepsilon_H)} \tag{11.5}$$

In order to calculate H concentrations from Eq. (11.5) the stopping cross section ε_M of the sample matrix at the probing depth can be obtained for example using SRIM (Chap. 11.2.1). It should be noted that for many compounds the stopping cross section is not very sensitive to details of the stoichiometry and the influence of uncertainties to the determination R_H is often small.

Though the constant K can be calculated from the resonance parameters and the detector efficiency it is in practice much easier and more reliable to obtain it from a measurement of a standard material with the known parameters $R_{H,s}$ and ε_s. Using Eq. (11.3) K is then

$$K = \frac{R_{H,s}}{Y_s \cdot \varepsilon_s} \tag{11.6}$$

This determination of K includes the calibration of the individual setup and it is good practice to check it from time to time. It should be emphasized however that nuclear reaction analysis is a method that needs a calibration only once because this calibration is valid for all types of samples and no standard is needed for an individual sample. This is a striking advantage of NRA compared to other analytical techniques such as for example Secondary Ion Mass Spectrometry (SIMS), where chemical and structural similar samples with known concentrations are needed for each sample type.

A numerical example for the calculation of a hydrogen concentration in a sample is given below in Sect. 11.2.7.

11.2.4   Depth Information

The depth information in a profile originates from the energy difference between the energy of the incident beam and the resonance energy. Since long the resonance is denoted as "the resonance at 6385 keV" though later measurements indicate a slightly higher value. A very precise measurement of the inverse reaction (i.e. the reaction of a proton beam with an ^{15}N sample) result in a value for an ^{15}N beam of (6393.6 ± 1.3) keV [14], another work reports the value of (6399.1 ± 2.9) keV [4]. In order to be independent from the absolute value of the resonance energy as well as from the absolute energy calibration of the accelerator one uses in practice a surface energy found in a measurement from a sample known to have surface hydrogen. The difference between surface energy and the energy at depth can then be converted by the stopping cross section into an areal atomic density (in units of atoms/cm^2) or an areal mass density. It is important to note that nuclear reaction analysis does not give the depth in length units (nm). To calculate this, the density of the sample has to be known which is not necessarily the density of bulk

material, in particular for thin layers or layered structures. Therefore, care has to be taken when thickness measurements of NRA are compared to analytical methods measuring the thickness of a sample layer directly in nm such as profilometric methods. In fact combining such results offers the option to determine densities. Nevertheless the description of layers in length units is often preferred in spite of uncertainties in the density since this is more vivid and ostensive.

For layered structures with significant different stopping cross sections the depth information over the entire system has to be calculated stepwise from the surface into the depth.

11.2.5 Depth Resolution

The depth resolution is ultimately limited by the width of the resonance used for depth profiling but for the narrow resonance at 6.4 MeV in the ^{15}N + H reaction other factors determining the depth resolution are dominant. One major contribution is the beam energy resolution ΔE_B, which is caused mainly by the high voltage ripple of the accelerator and the charge state of the ion beam used. It is determined eventually by the energy defining elements of the accelerator such as slits at the analyzing magnet. Detailed studies can be found in [15, 16]. At a tandem accelerator the beam resolution is usually between 5 and 10 keV for a 6.4 MeV nitrogen beam but for many accelerators it is not known exactly. It is not worthwhile to investigate and improve the beam resolution much further unless sophisticated cryogenic techniques for the sample are employed because another factor determining the depth resolution is the Doppler broadening [15, 17] which is due to thermal motion of the sample atoms. Though thermal energies are much smaller than the energy of the ion, the effective energy for the hydrogen atom is given by

$$E_{eff} = \frac{1}{2}M(\mathbf{v}_N + \mathbf{v}_H)^2 \tag{11.7}$$

where M is the mass of the projectile (here ^{15}N) and $\mathbf{v}_N$ and $\mathbf{v}_H$ the velocity vectors of the beam and the hydrogen atom respectively. Though $\mathbf{v}_H$ is negligible compared to $\mathbf{v}_N$ the mixed term of this quadratic addition is not and—since $\mathbf{v}_H$ is randomly distributed in space—gives rise to a distribution which is well approximated by a Gaussian with a FWHM of

$$\Delta E_D = 4\sqrt{\frac{\ln 2\ ME\ k_B T}{m}} \tag{11.8}$$

Here E is the energy of the beam, k_B the Boltzmann constant, T the temperature and m the mass of the sample atom (here hydrogen). This formula is in principle correct for free hydrogen atoms (or noble gases) only, in cases of molecules and/or lattices corrections have to be applied, which can be complicated [18, 19] and give

rise to significant larger values than obtained by Eq. (11.8). In fact several groups [20, 21] used the Doppler broadening to study the hydrogen bonding in gases or at solid surfaces. The width of the Doppler broadening depends on the sample material and is around 10 keV.

Like the Doppler broadening the beam resolution can be approximated by a Gaussian as well. Both influences add quadratically to the experimental resolution

$$\Delta E_{exp} = \sqrt{\Delta E_D^2 + \Delta E_B^2} \qquad (11.9)$$

To get the total resolution this Gaussian needs to be convoluted with the resonance shape, which is a Breit-Wigner curve (i.e. a Lorentzian) resulting in a Voigt profile. This distribution is centered around the resonance energy, its width cannot be calculated analytically and is between a linear and quadratic summation of the Gaussian and Lorentzian components. Details can be found in [15].

For the case of an ^{15}N beam and the resonance at 6.4 MeV the total resolution is dominated by the experimental resolution since the resonance is so narrow. From the discussion above one can estimate an achievable energy resolution between 10 and 20 keV. Such values are found in practice in many laboratories and correspond to a depth resolution e.g., in silicon between 7 and 14 nm and in tungsten between 2.5 and 5 nm. This information is sufficient for many applications where structures with much larger thicknesses are investigated.

In cases where the exact resolution needs to be known, e.g. when layer thicknesses are in the range of the resolution one has to study experimentally the so-called instrument function. This is essentially the shape of the yield curve for a monatomic or very thin hydrogen layer. For this, a sample with low hydrogen concentration in the bulk but a defined surface layer is needed. There are several materials possible such as silicon wafers, W samples or even standard Al household foil [6], which is known to have very low hydrogen content. The main experimental challenge is here to maintain a defined surface layer during the measurement, which requires a very good vacuum in the UHV regime to avoid hydrogen build up by adsorption from the vacuum or beam induced deposition of Carbon on the surface. The experimental details will be discussed in Sect. 11.3.5.

Figure 11.3 shows a yield curve of a thin hydrogen layer on a silicon wafer measured with the set up employed at present at the tandem accelerator of the University of Bochum. The data points have been fitted with a Gaussian distribution only since the influence of the resonance width is negligible. The fit leads to a full width at half max of (13.9 ± 0.3) keV. If the layer is thinner than the width of the instrument function the hydrogen concentration and depth cannot be calculated anymore, as discussed above. Here the yield curve has to be analyzed differently, details of which are beyond the scope of this book and can be found in [22]. With this somewhat more complicated analysis one can determine the areal density of a thin hydrogen layer, which is for the data in Fig. 11.3 $1.9 \cdot 10^{15}$ atoms/cm^2 and therefore in the monolayer range only.
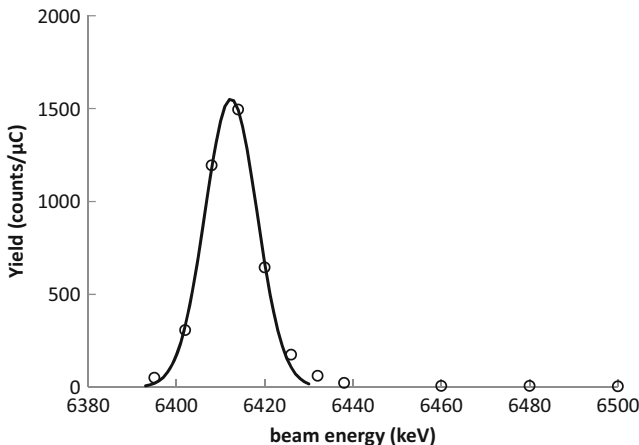
Fig. 11.3 Yield curve of a layer of hydrogen in the monolayer range on Si as an example for an instrument function

11.2.6 Straggling

The depth resolution discussed so far is valid in near surface regions only. In larger depth the energetic beam width deteriorates due to the statistical nature of the energy loss process. This effect is called the energy straggling ΔE_S and needs to be taken into account for larger energy losses e.g. when interfaces in larger depth are studied. It can be estimated qualitatively by Bohr's formula [23], which is a good approximation for a ^{15}N beam at the energies of relevance here.

$$\Delta E_S = 2\sqrt{2 \cdot \ln 2} \cdot \sqrt{4\pi \ e^2 \ Z_1^2 \ Z_2 \ N} \tag{11.10}$$

with e being the elementary charge, Z_1 and Z_2 the atomic number of the projectile and the sample atoms, respectively and N the thickness of the layer the beam has penetrated. It is noteworthy that this approximation is independent of the energy of the projectile. In numerical values one gets $E_S = 1.2 \cdot \sqrt{Z_1^2 \ Z_2 \ N}$ in keV, when the layer thickness is given in 10^{18} atoms/cm^2. So, for a 100 nm thick Si layer which is $0.5 \cdot 10^{18}$ atoms/cm^2 one gets $\Delta E_S = 22.2$ keV (i.e. 16 nm), a 1 μm layer would result in a straggling of 70 keV (i.e. 50 nm). These values have to be added quadratically to the energy resolution discussed above. For compounds the straggling of each component has to be added quadratically [5]

A summary of more refined theoretical descriptions of the straggling can be found e.g. in [5]. A very practical way (e.g. for layers containing compounds or layered structures) to calculate the straggling is to use the SRIM program, which is not only a source for tabulated stopping power values but can also do a sophisticated Monte Carlo simulation of the energy loss process. After entering thickness,
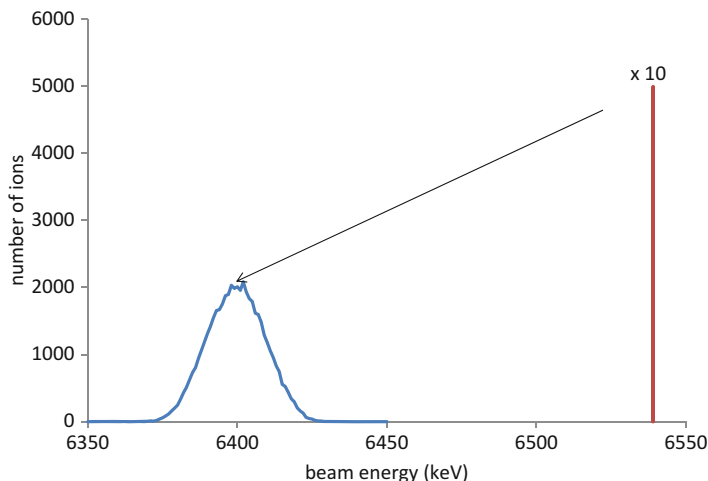
Fig. 11.4 Monte Carlo SRIM simulation of the energy broadening of a monoenergetic ^{15}N beam of 6.54 MeV after penetrating 100 nm of silicon

stoichiometry and density of one or more layers penetrated by the beam the program has the option to calculate the energies of the transmitted ions. If these values are binned appropriately one gets a distribution such as displayed in Fig. 11.4. The initial energy has been chosen such that the distribution of the transmitted ions is centered around the resonance energy of 6.4 MeV after passing 100 nm of silicon. The width of this distribution is 23.6 keV, which is in good agreement with the value of 22.2 keV from Bohrs approximation.

Finally it should be mentioned that a broadening of a slope of a hydrogen concentration can be caused not only by straggling but also by cases when a layer thickness is inhomogeneous within the area of the beamspot which will have a similar effect on the hydrogen concentration profile.

11.2.7   A Simple and Straightforward Example

As an example for the measurement of a depth profile we discuss here a study carried out in the course of a research program dealing with hydrogen storage materials [24, 25]. This example is simple and straightforward in the sense that the samples proved to be stable during the measurements (see discussion below) and the hydrogen concentrations are high.

The depth profiling has been performed with a setup used at present at the Ruhr-University of Bochum (Fig. 11.5) and described in more detail in [22]. It is designed for the measurement of low hydrogen concentrations, which will be discussed in Sect. 11.3.5. In brief, the beam enters the main chamber via a pipe with 2 mm in
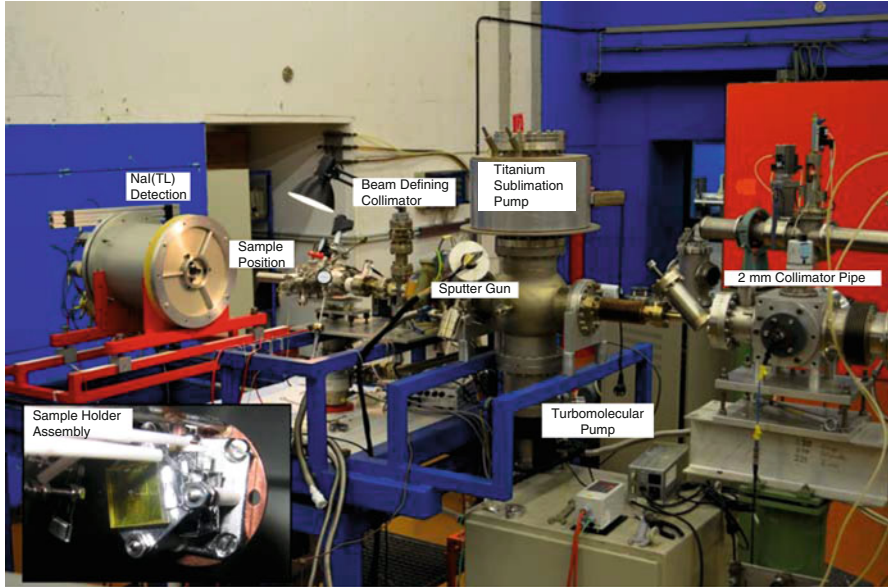
Fig. 11.5 Photograph of the setup at the Ruhr-University Bochum and (*inset*) details of the sample holder assembly with a ZnO-crystal mounted (see text)

diameter and a length of 10 mm, which serves also to separate the UHV in the chamber from the standard vacuum in the accelerator beam line ($\approx 10^{-6}$ mbar). The beam is then defined by a collimator of 1 mm or 3 mm in diameter, 60 cm in front of the sample position to avoid contributions from possible hydrogen contaminations in the collimator material. The sample is placed at the end of a pipe, which can be entirely surrounded by a 30 cm × 30 cm NaI(TL) borehole detector, which has a photopeak detection efficiency of 48 % for the 4.4 MeV γ-ray. The K factor for this arrangement as defined in Sect. 11.2.3, Eq. (11.6) has been determined in various measurements from standard samples with known hydrogen concentrations to be $7.10 \cdot 10^7 \, \mu C/(eV \, cm^2)$.

Sample layers of Yttrium were produced by magnetron sputtering onto a SiO_2/Si substrate. These samples were loaded with hydrogen inside the sputter chamber with forming gas (95 % Ar/5 % H_2) for 1 h. This was done either in-situ at room-temperature directly after the deposition or after exposure to air and at a temperature of 500° C. Depth profiles for the two types of samples are shown in Fig. 11.6. In the upper part of Fig. 11.6 the raw data are plotted as the γ-yield per particle μC and in the lower part the hydrogen concentration is calculated according to the formalism given in Sect. 11.2.3. One can clearly see that the slopes between Fig. 11.6a, b are different because the varying stopping power due to the changing hydrogen concentration has been taken into account. The measurements have been carried out with a beam intensity of 10–20 nA, the total time needed for one depth profile was about 2 h.
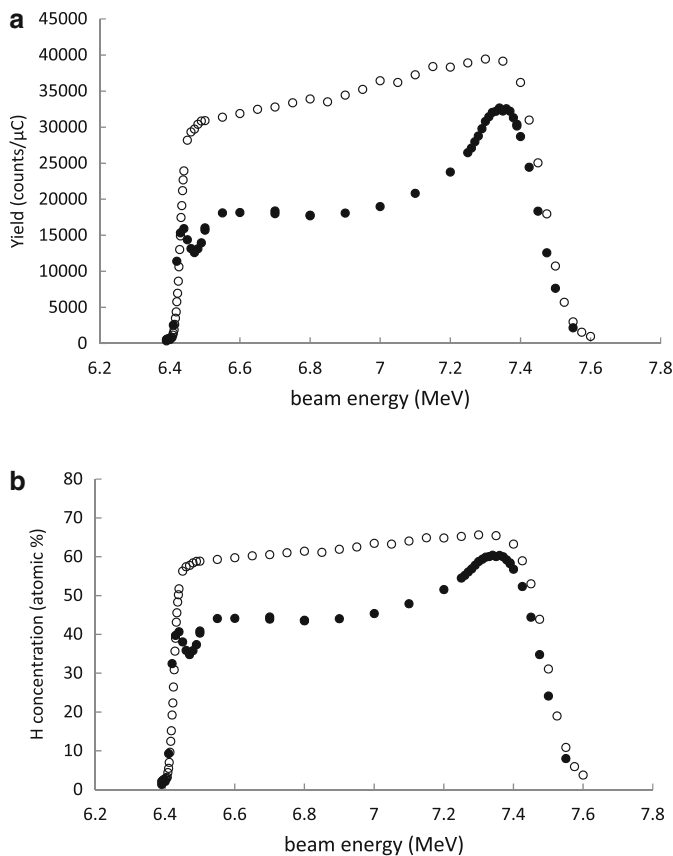
Fig. 11.6 Yield (**a**) and hydrogen concentration R (**b**) of Y layers loaded in-situ after deposition (*open circles*) and loaded after exposure to air (*solid points*)

In order to give a numeric example for the calculation of a hydrogen concentration outlined in Sect. 11.2.3 we select the point measured at 7 MeV for the sample exposed to air. Here 11290 γ-rays have been measured with a particle beam charge of 0.6 µC. The yield is therefore $1.88 \cdot 10^4$ counts/µC. The stopping cross sections of yttrium and hydrogen at 6.4 MeV are $566 \cdot 10^{-15}$ and $60.9 \cdot 10^{-15}$ eV $\cdot$ cm², respectively. Note that even though the beam energy is 7 MeV the stopping power at the resonance energy is relevant because the γ-rays are produced in the depth, where the ions have 6.4 MeV.

With these numbers and the K-factor given above Eq. (11.3) leads to R = 76 %, while Eq. (11.5) yields R = 45 %. This shows exemplarily the necessity to include the hydrogen in the calculation of the stopping power, when measuring high hydrogen concentrations.

For the sample loaded in-situ one gets an almost homogeneous hydrogen concentration over the entire thickness of the layer while for the sample loaded after exposure to air the hydrogen storage capacity is significantly reduced. In

addition one can identify a surface peak, which arises from a layer adsorbed from the ambient air.

The energy difference of the 50 % points of the rising and falling edge of the depth profile for the in-situ loaded layer is here 1074 keV. Assuming an average hydrogen concentration of 60 % and therefore a stopping power of 263 eV/(10^{15} atoms/cm^2) throughout the layer, the thickness is then $4.09 \cdot 10^{18}$ atoms/cm^2 of Y and H atoms together. In this case it is very uncertain to convert this into length units, because the density of the layer after loading is very uncertain. Additionally the layer is partly oxidized (as found by RBS measurements), which would have to be included in the stopping power calculation. Assuming the literature value for the density of yttrium the thickness would be 1.35 μm but most probably it is significantly smaller.

11.3 More Special Cases and Complications

While the example discussed above illustrates the simplicity of the measurement and the analysis of the data one has to be aware that complications and difficulties come along with certain samples, which require additional efforts for the experimental set up and the analysis of the data. One crucial point in each measurement is the stability of the samples under beam irradiation. Another important issue is the detection of low hydrogen concentrations which requires a closer look at the γ-ray detection, a discussion of background and the problems arising when measuring low concentrations in a certain depth while high concentrations are present at other depths or at the surface.

Measuring low hydrogen concentrations is important since hydrogen can change the properties of materials significantly even at low concentrations. Many efforts have been undertaken in the past to measure small traces of hydrogen. A prominent example is the determination of hydrogen in minerals of the Earth's crust and mantle such as olivine. Here, concentrations in the range of a few at. ppm have strong impacts on the mechanical properties such as viscosity and melting point behavior of rocks containing these minerals, which are crucial for an understanding of geodynamics [26]. Moreover, the hydrogen content in the so-called nominal anhydrous minerals (NAMs) may be an important contribution in the water balance of the earth mantle and could exceed the water stored in the oceans [27].

Although there are analytical techniques to measure low hydrogen concentrations such as IR spectroscopy (FTIR), these techniques need to be calibrated for the determination of absolute quantities. Remarkable work in the field of geoscience on the calibration of hydrogen concentrations down to a level of 10 at. ppm has been done in the past [28, 29]. A setup dedicated for the measurement of concentrations in the at. ppm region with NRA is described in [6]. In the following the experimental challenges and requirements to be fulfilled for such analyses are discussed in more detail.

11.3.1 Stability of Samples Under Irradiation

Sometimes the question arises about the change of the hydrogen concentration in a sample by the detecting nuclear reaction, which converts the hydrogen with the beam ion into a ^{12}C atom and an alpha particle. It is easily understood, however, that with atomic densities of materials in the order of 10^{22} atoms/cm^3 a layer of about 10 nm thickness as probed by the resonance has still 10^9 hydrogen atoms/cm^2 at a hydrogen concentration of 1 at. ppm. If a beam has a diameter of 1 mm^2 there are 10^7 hydrogen atoms available for the detection. Considering a detection efficiency of some 50 % the conversion of 10^3 hydrogen atoms by the nuclear reaction, i.e. four orders of magnitude less, would lead to an excellent counting statistics in the γ-peak, disregarding whether this can be accomplished in reasonable time for such a low concentration. Therefore the "consumption" of hydrogen by the detecting reaction is always negligible.

Nevertheless the stability of samples under irradiation is an important issue and it is mandatory in each study to prove that samples are stable or that the deterioration of the hydrogen concentration is understood and corrected for. Changes in the concentration can be caused by various effects of the beam such as structural or chemical changes by the ions or just by warming up the samples due to the power deposited by the beam. This power can be easily calculated by multiplying the energy of the ions with the number of ions per time, which is the electrical beam current divided by the charge state of the ions (in units of the elementary charge e). For example a nitrogen beam of ions with charge state 3 e and a beam intensity of 30 nA at an energy of 6.4 MeV results in a power of 64 mW, which needs to be dissipated by the sample.

Therefore, the deterioration of the hydrogen concentration can be dependent on both, the fluence, which is the number of ions per cm^2 accumulated during a measurement ("how long and how many points have been measured?") and on the beam intensity i.e. number of ions per seconds ("how fast has been measured?"). Sometimes samples reach a stable level after an initial degradation, which can be an indication that hydrogen is present in different phases. For specific applications detailed studies can be found in literature such as the early work of Thomas et al. [30].

Fortunately many layers are stable or change only little under beam irradiation in particular when a detector with high detection efficiency is employed or the beam can probe a larger area on the sample. Both approaches lead to a smaller beam load per sample area and thus to smaller deterioration effects. However, some samples are very sensitive to the beam and a detailed study of the effect of hydrogen loss is needed to be able to gain at least some information about depth profiles.

We present here an example related to cosmochemistry studies. Hydrothermal serpentinization experiments of amorphous silicates (FeMgSiO$_4$) are performed to constrain the conditions of alteration (temperature, timescale) of such silicates in asteroids, where they reacted with water at the time of the solar system formation. In these experiments, amorphous silicates react with water at a temperature

between 50 and 150° C and amorphous hydrated silicates are formed. This leads to a hydrogen (water) containing layer structure at the minerals surface in the depth range of μm and NRA is used to obtain hydrogen depth profiles. Details and results of these studies can be found in [31, 32].

These samples are very sensitive to beam damage and a reference material (natural serpentine; water content ≈ 14 mol%) was used to determine empirically a law for the hydrogen loss behavior and ultimately apply this law to real experimental samples. To probe the hydrogen loss at a certain depth the beam energy was set to 6.7 MeV. First the hydrogen content was measured with a low beam current of 0.8 nA for a time of about 1 min. This was repeated several times. The loss of hydrogen as a function of the total beam charge accumulated on the sample is shown in Fig. 11.7a. Then the beam current was progressively increased. One finds that the hydrogen loss (i.e. the difference between the measured and the initial concentration) follows a steady trend, which can be fitted with a logarithmic function of the fluence i.e. the accumulated charge. Above beam currents of 100 nA, the hydrogen loss rate increases indicating that further mechanisms such as warming-up by the beam intensity come into play.

The data from Fig. 11.7a corrected with the obtained loss function are shown in Fig. 11.7b. The hydrogen concentration is converted into a water concentration assuming that hydrogen is present in the layer in form of water only. One can see that the logarithmic correction works well within the statistical errors up to a beam current of 12 nA; under this condition depth profiles can be gained.

11.3.2 High Efficiency γ-Ray Detection

In order to measure low hydrogen concentrations it is crucial to detect the γ-rays with high efficiency. As pointed out above this is not only necessary for a high sensitivity but also advantageous for sensitive samples, which can then be measured with low beam current. Hence, a large detector is needed which is ideally a borehole detector with the sample in its center thus covering a large solid angle. Since the detector resolution is of minor importance, scintillation detectors are favorable. Typical detectors are sodium iodide (see Fig. 11.5) or bismuth germanate (BGO) detectors [6]. Barium fluoride as detector material has the disadvantage of an intrinsic background. While NaI(Tl) detectors have a slightly better energy resolution, BGO detectors are smaller in size for the same efficiency, which can be important for the design of a background shielding. Another issue in the design of a high efficiency setup is that the constructive elements of the sample holder assembly and vacuum chamber should be designed such that absorption of γ-rays on their path from the sample to the detector is minimal.
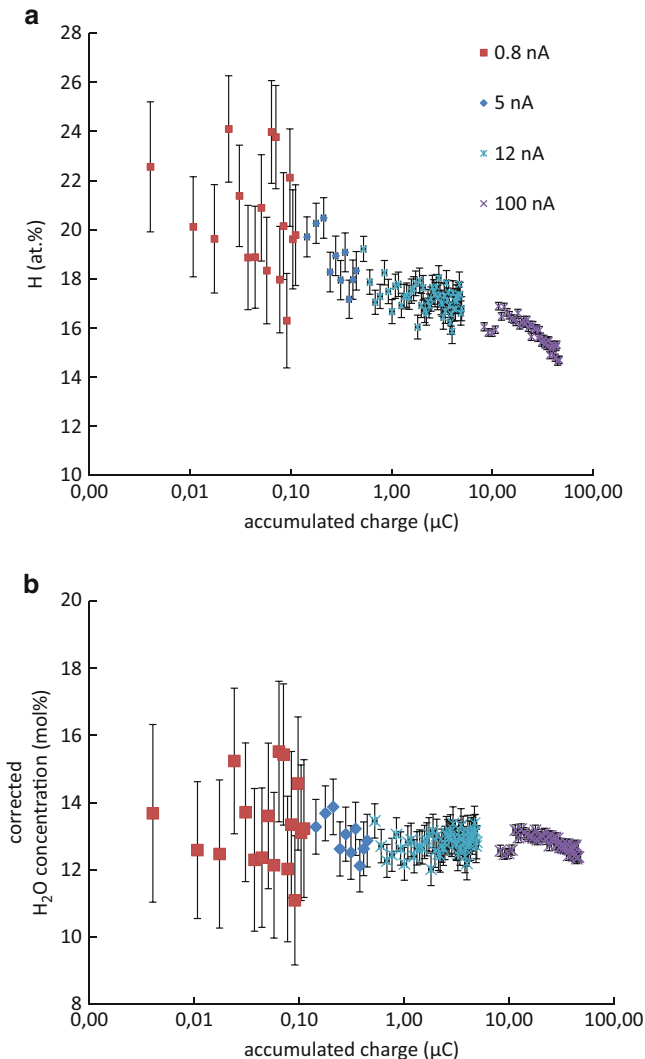
Fig. 11.7 (**a**) Hydrogen loss in serpentine induced by the beam measured with increasing intensities (**b**) water content deduced from (**a**) after correction for the loss

11.3.3   Background

When measuring the γ-yield of the 4.4 MeV line one has to consider background counts in the region of interest (see spectrum in Fig. 11.2), in particular for low hydrogen concentrations. Background can arise from the room, cosmic rays, the accelerator, and in the beam transport system as well as from contributions produced in the sample itself.

The room background is due to natural radio nuclides in ambient materials, mainly the γ-activity of ^{40}K and ^{208}Tl of building materials like concrete or bricks. The corresponding γ-ray lines of 1461 and 2614 keV can clearly be seen in the spectrum in Fig. 11.2. Although these lines are below the region of interest of the hydrogen signal their intensity can be high in environments with a high amount of concrete, which is typical for accelerator buildings. Then a summing of two simultaneously occurring events (pile up) leads to counts in the region of 4.4 MeV. This effect can be reduced only by a lead shielding of the detector with a thickness of at least 5 cm.

Cosmic rays, mainly muons, cause a smoothly sloping background level all over the spectrum and are the dominant contribution at energies higher than the room background. Unfortunately a lead shielding against the room background increases the height of the cosmic background by secondary rays from the shielding material. Muons and their secondary γ-rays can be suppressed by an active shielding. This is usually a scintillator surrounding the detector, which detects the muons and can veto the erroneous event in the γ-detector. Both shieldings together allow background suppressions roughly in the order of one magnitude.

Since the intensity of the room background and the muons is dependent on the acquisition time only, its influence is smaller when the measurements can be done with high beam intensity. In practice accelerators can provide beam currents from below 1 nA to several hundreds nA or even more. This corresponds to a change in the signal to background ratio over more than two orders of magnitude. The limiting factor is here the stability of the sample as discussed in Sect. 11.3.1. Therefore in general, the sensitivity to low concentrations is not attributed to the experimental setup only, but also depends strongly on the sample stability.

Background induced by the beam hitting the constructive elements of the setup is another source for a spurious contribution to the γ-spectra. This is in particular true for the beam defining collimators, which must be manufactured out of low hydrogen containing material. However, most surfaces even under UHV conditions will adsorb over time a hydrogen bearing layer, which are a source of unwanted signals. There are several technical solutions to overcome this problem such as heating the collimators [6]. Another approach is to mount the last beam defining collimator that far in front of the detector position (see for example Fig. 11.5) that the efficiency for detecting γ-rays from there is small. In practice, that is half a meter or more which, however, makes the size and position of the beam on the sample less defined and puts some constrains on the minimal sample size. For the setup in Fig. 11.5 for example the minimum sample size is 3 mm in diameter.

Beside these sources of background the accelerator and beam transport system can be a source of neutrons. If those neutrons reach the detector, neutron capture reactions with the detector material will produce interfering detector signals.

Another source of background coming from the sample itself can arise from nuclear reactions of ^{15}N ions with other nuclides than hydrogen. One relevant case is the reaction with deuterium, which produces several γ-ray lines possibly interfering with the region of interest around 4.4 MeV. Therefore, care has to be taken when deuterated materials are studied and a subtraction of background induced by deuterium has to be applied.

11.3.4   Samples with Hydrogen Concentrations Strongly Varying with Depth

When samples have a hydrogen concentration depth profile which changes over several orders of magnitude the assumption of a detection window only at the resonance energy is not valid any more. Then the non-resonant cross section (Fig. 11.1) will contribute to the reaction yield. For example if a layer with a higher hydrogen concentration is deposited on a substrate with very low concentration and the hydrogen in the substrate is probed, the non-resonant yield from the layer might be equivalent to the yield at the resonance window in the substrate. In those cases one has to measure the hydrogen concentration in the layer and calculate from the total (integrated) hydrogen present in the layer the non-resonant yield in measurements of the substrate. This is the product of the hydrogen areal density of the layer multiplied by the non-resonant cross section and the detector efficiency. For example, if the thickness of the layer is measured to be 10^{17} atoms/cm2 and the mean hydrogen concentration is 10 at. %, then the number of hydrogen atoms is 10^{16} atoms/cm^2. The cross section for a non-resonant contribution at a beam energy of e.g. 7 MeV is about 0.1 mbarn (Fig. 11.1) . This leads to a probability of $5 \cdot 10^{-13}$ counts per incident particle or about 3 counts per particle μC beam charge, assuming a detector efficiency of 50 %.

The problem of the non-resonant yield becomes important also when hydrogen concentrations in the at. ppm range are to be measured. Then hydrogen containing surface layers, almost always found on sample surfaces, will contribute to the yield. As an example, the influence of a surface layer containing 10^{16} hydrogen atoms/cm^2 (about 10 monatomic layers only) is simulated for a measurement of hydrogen-free silicon with the set-up at Bochum (Fig. 11.8). It can be seen that already at
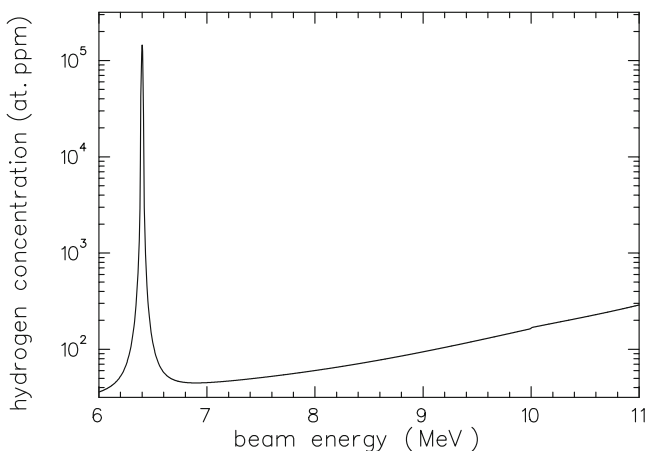

Fig. 11.8 Influence of a hydrogen surface layer of 10^{16} atoms/cm^2 on measurements at greater depth for a hydrogen free material (Si) due to non-resonant contribution

7 MeV the surface layer feigns some 30 at. ppm hydrogen and at greater depth the effect exceeds 100 ppm.

As a consequence, investigating such low concentrations requires an ultra-high vacuum in the region of 10^{-9} mbar or better and measures such as surface cleaning. Surface cleaning can be done by e.g. conventional low energy ion sputtering and/or heating the sample [22, 33]. A commercial sputter gun for surface cleaning installed at the setup in Bochum can be seen in Fig. 11.5. Sometimes surface cleaning is done for simplicity with the analyzing ^{15}N beam at higher beam currents. However, cleaning with a high energy beam comes along with a damage of the sample at greater depth.

11.3.5 Example of Low Concentration Detection

To illustrate the results and limits for a measurement of hydrogen concentrations we present here measurements on ZnO single crystals [22]. ZnO is an interesting material in a number of applications, like in the fields of optoelectronics and semiconductors as well as in heterogeneous catalysis. In this framework an understanding of hydrogen adsorption on single crystal surfaces as well as the determination of the native hydrogen bulk concentration is important.

It turned out, that unprepared ZnO surfaces have a surface coverage of unspecified hydrogen compounds and a well-defined preparation of the sample is an essential requirement for these studies. A clean single crystal surface can be prepared in-situ by several cycles of low energy ion sputtering and subsequent heating and annealing of the surface. With this procedure a H surface coverage in the order of 10^{14} at/cm^2 can be achieved which was slowly increasing to $6 \cdot 10^{14}$ at/cm^2 (one atomic monolayer of ZnO) due to hydroxylation from the residual gas ($\approx 10^{-9}$ mbar). Under this condition studies of H adsorption and hydroxylation at the ZnO surface in the range of one atomic layer are feasible. Additionally, these conditions minimize the spurious non-resonant contribution when measuring the low concentration of the crystal bulk. It should be noted that for this type of measurements sample preparation takes several days and therefore much more time than the measurements with the ion beam itself.

The results for the surface studies can be found in [22]; we show here the result of bulk measurements. As an example, a γ-spectrum taken at a depth of 160 nm in ZnO is displayed in Fig. 11.9. Extensive studies before showed that the bulk hydrogen concentration did not change due to beam deterioration even at beam intensities up to 100 nA particle current. The spectrum in Fig. 11.9 has been obtained with this beam intensity in about 5 min (red curve). A typical bulk concentration of ZnO was determined from such a spectrum to be 300 at. ppm with a variation of $+/-$ 100 at. ppm for different crystals. In order to explore background contributions from the collimators a background spectrum has been taken with the same beam charge but with Al household foil as a sample (black curve). This spectrum illustrates the sensitivity for this measurement and allows estimating the detection limit in this case to less than 100 at. ppm.
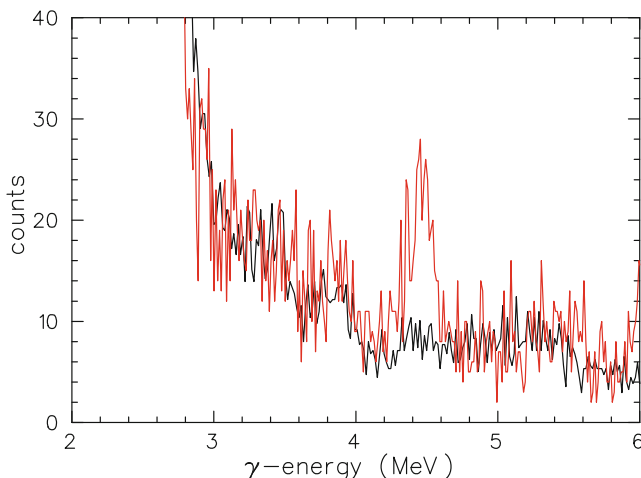
Fig. 11.9 The gamma spectrum of the ZnO bulk concentration shows a clear signal of hydrogen in a depth of 160 nm (*red*). The signal intensity corresponds to a H concentration of 300 at. ppm. The background level (*black*) is represented by a blank measurement of aluminum, which is known to have a hydrogen content of few at. ppm only [6]

References

1. D.A. Leich, T.A. Tombrello, Nucl. Instrum. Methods **108**, 67 (1973)
2. W.A. Lanford, H.P. Trautvetter, J.F. Ziegler, J. Keller, Appl. Phys. Lett. **28**, 566 (1976)
3. W.A. Lanford, Nucl. Instrum. Methods **B66**, 65 (1992)
4. H.W. Becker, M. Bahr, M. Berheide, L. Borucki, M. Buschmann, C. Rolfs, G. Roters, S. Schmidt, W.H. Schulte, G.E. Mitchell, J.S. Schweitzer, Z. Phys. A **351**, 453 (1995)
5. Y. Wang, M. Nastasi (eds.), Handbook of Modern Ion Beam Materials Analysis, 2nd edn. (Materials Research Society, Pittsburgh, 2009). ISBN 978-1-60511-215-2
6. D. Endisch, H. Sturm, F. Rauch, Nucl. Instrum. Methods **B84**, 380 (1994)
7. M. Wilde, K. Fukutani, Surf. Sci. Rep. **69**, 196 (2014)
8. J.F. Ziegler, SRIM, The Stopping and Range of Ions in Matter (2013), http://www.srim.org/SRIM/Compounds.htm
9. J.F. Ziegler, M.D. Ziegler, J.P. Biersack, Nucl. Instrum Methods **B268**, 818 (2010) http://www.srim.org
10. K.M Horn, W.A. Lanford, Nucl. Instrum Methods **B34**, 1 (1988)
11. G. Imbriani, R.J. deBoer, A. Best, M. Couder, G. Gervino, J. Görres, P.J. LeBlanc, H. Leiste, A. Lemut, E. Stech, F. Strieder, E. Uberseder, M. Wiescher, Phys. Rev. C **85**, 065810 (2012)
12. B. Maurel, G. Amsel, Nucl. Instrum Methods **218**, 159 (1983)
13. W. Rudolph, C. Bauer, K. Brankhoff, D. Grambole, R. Grötzschel, C. Heiser, F. Herrmann, Nucl. Instrum Methods **B15**, 508 (1986)

14. T. Osipowiez, K.P. Lieb, S. Brüssermann, Nucl. Instrum Methods **BI8**, 232 (1987)
15. G. Amsel, B. Maurel, Nucl. Instrum Methods **218**, 183 (1983)
16. L. Borucki, H.W. Becker, F. Gorris, S. Kubsky, W.H. Schulte, C. Rolfs, Eur. Phys. J. A **5**, 327 (1999)
17. W.H. Schulte, H. Ebbing, S. Wüstenbecker, H.W. Becker, M. Berheide, M. Buschmann, C. Rolfs, G.E Mitchell, J.S. Schweitzer, Nucl. Instrum Methods **B71**, 291 (1992)
18. W.E. Lamb, Phys. Rev. **55**, 190 (1939)
19. J.M. Donhowe, J.A. Ferry, W.G. Monrad, R.G. Herb, Nucl. Phys. **A102**, 383 (1967)
20. M. Zinke-Allmang, O. Kruse, Nucl. Instrum Methods **B90**, 579 (1994)
21. K.M Horn, W.A. Lanford, Nucl. Instrum Methods **B29**, 609 (1988)
22. F. Traeger, M. Kauer, Ch. Wöll, D. Rogalla, H.W. Becker, Phys. Rev. B **84**, 075462 (2011)
23. N. Bohr, K. Dan Viden, Selsk. Math. Fys. Medd. **18**, 1 (1948)
24. A. Ludwig, J. Cao, B. Dam, R. Gremaud, Appl. Surf. Sci. **254**, 682 (2007)
25. A. Ludwig, J. Cao, A. Savan, M. Ehmann, J. Alloys Compd. **446–447**, 516 (2007)
26. G. Hirth, D.L. Kohlstedt, Earth Planet. Sci. Lett. **144**, 93 (1996)
27. M. Murakami, K. Hirose, H. Yurimoto, S. Nakashima, N. Takafuji, Science **295**, 1885 (2002)
28. D.R. Bell, G.R. Rossmann, J. Maldner, D. Endisch, F. Rauch, J. Geophys. Res. **108**(B2), 2105 (2003)
29. J. Gose, P. Reichart, G. Dollinger, E. Schmädicke, Am. Mineral. **93**, 1613 (2008)
30. J.-P. Thomas, M. Fallavier, J. Tousset, Nucl. Instrum. Methods **187**, 573 (1981)
31. C. Le Guillou, H.G. Changela, R. Dohmen, T. Müller, A.J. Brearley, C. Vollmer, D. Rogalla, H.W. Becker, Contribution to the 45th Lunar and Planetary Science Conference, The Woodlands
32. C. Le Guillou, R. Dohmen, D. Rogalla, T. Müller, C. Vollmer, H.-W. Becker, Chem. Geol. Chem. Geol. **412** (2015) 179
33. J. Maldner, F. Rauch, AIP Conf. Proc. **392**, 689 (1997)